Synchronous change of atmospheric CO_2 and Antarctic temperature during the last deglacial warming

Authors: F. Parrenin[1*], V. Masson-Delmotte[2], P. Köhler[3], D. Raynaud[1], D. Paillard[2], J. Schwander[4], C. Barbante[5,6], A. Landais[2], A. Wegner[3] and J. Jouzel[2]

Affiliations:
[1]Laboratoire de Glaciologie et Géophysique de l'Environnement (CNRS/UJF), Grenoble, France.
[2]Laboratoire des Sciences du Climat et de l'Environnement (CEA/CNRS/UVSQ-IPSL), Gif-sur-Yvette, France.
[3]Alfred Wegener Institute for Polar and Marine Research, Bremerhaven, Germany.
[4]Physics Institute, University of Bern, Bern, Switzerland.
[5]Department of Environmental Sciences, University of Venice, Venice, Italy.
[6]Institute for the Dynamics of Environmental Processes - CNR, University of Venice, Venice, Italy
*Correspondence to: parrenin@ujf-grenoble.fr

Abstract: Understanding the role of atmospheric CO_2 concentration (hereafter aCO_2) during past climate warmings requires clear knowledge of how it varies in time relative to temperature. Antarctic ice cores preserve highly resolved records of aCO_2 and Antarctic temperature (AT) for the last 800 kyr. Here we propose a revised relative age scale between aCO_2 and AT for the last deglacial warming (Termination I, TI) using data from 5 Antarctic ice cores. We infer the phasing between aCO_2 and AT at four times when their trends change abruptly. We find no significant lead/lag, with a 1σ accuracy ranging from 160 yr to 90 yr, indicating that aCO_2 did not begin to rise hundreds of years after Antarctic temperature, as has been suggested by earlier studies.

One Sentence Summary: A new chronology shows that changes in atmospheric CO_2 and Antarctic temperature were synchronous during the last deglacial warming.

Main Text: The most highly resolved aCO_2 record during TI has been obtained so far from the EPICA Dome C (EDC) ice core*1, 2*. In this record, aCO_2 appears to lag local temperature by 800±600 years at the onset of TI, in agreement with an earlier study on the Vostok and Taylor Dome ice cores which identified a lag of 600±400 years at the end of the last three terminations*3*. However uncertainties in the relative timing of aCO_2 and AT remain for two reasons. First, air is trapped in fallen snow only when it has recrystallized enough to create enclosed cavities, typically at a depth of 50-120 m below the surface (depending on site conditions), at the bottom of the so-called firn. This results in a depth difference (Δdepth, see Figure 1) between synchronous events recorded in the ice matrix and in the trapped gas bubbles/hydrates*4, 5*. Here we will use air $\delta^{15}N$ data from the EDC ice core to determine the past Lock In Depth (LID). The LID estimates are transformed to Δdepth estimates using a constant firn average density and a modeled vertical thinning

function. Our approach is further validated with 2 independent methods. Second, using only the isotopic record from one ice core produces a noisy reconstruction of past temperature variations in Antarctica. Here we will use a stack of Antarctic temperature variations based on 5 synchronized ice cores.

Figure 2 illustrates an approach similar to previous studies*1, 3* to deduce Δdepth, based on firn densification modeling*6* to estimate the past LID and average firn density, and ice flow modeling*7* to estimate the vertical thinning of ice layers. The past LID can also be estimated using the fact that in the firn, below a convective zone where the air is freely mixed, gravitational fractionation enriches the $\delta^{15}N$ of N_2 proportionally to the height of the diffusive column*8, 9*. There is no convective zone today at EDC*10*. Assuming a persistent absence of such a convective zone during TI and using the $\delta^{15}N$ data from the EDC ice core*11*, we can estimate the LID during TI. Then, assuming the average firn density did not vary and using a 1-D ice flow model*7* to assess layer thinning, the LID can be converted to Δdepth (Figure 2 and Supporting Online Material, SOM).

One caveat of our method arises from our assumed absence of a convective zone during the past, which is known to reach more than 20 m in low accumulation, windy sites today*12*.

For verification, we use 2 independent approaches. First, we synchronize EDC to the EPICA Dronning Maud Land (EDML) and Talos Dome (TALDICE) ice cores both in the gas (using CH_4) and ice (using volcanic events) phases*5*. Δdepth at EDC can be estimated from Δdepth at EDML and TALDICE (Figure 1). The latter is evaluated from firn modeling but, because the accumulation is ~3 times higher at EDML or TALDICE than at EDC, an error on the past LID at EDML or TALIDCE has a ~3 times smaller impact at EDC*5*.

Second, we use the bipolar seesaw hypothesis*13*, which suggests that a rapid temperature rise (fall) in Greenland occurs synchronous to a maximum (minimum) in Antarctic temperature. This hypothesis has been proven by relative dating of ice cores around the Laschamp geomagnetic event*14*. Here, we assume that the fast CH_4 transitions in EDC can be taken as proxies of rapid Greenland temperature changes, thus revealing three tie points during TI (Figure 3). The fact that it is possible, with a very simple mathematical model*15*, to construct from the EDC ice isotope record a Greenland-like temperature time-serie, correctly capturing stadial-interstadial transitions (corresponding to the extrema of the EDC ice isotope record) make it very likely that the bipolar seesaw pattern is robust within the duration of these rapid transitions. These independent methods, either based on the synchronization of EDC to EDML and TALDICE or on the bipolar seesaw hypothesis, confirm our $\delta^{15}N$ method for TI within their 1σ confidence intervals, suggesting that the convective zone indeed was absent or nearly absent during TI at EDC.

We therefore build a new gas chronology based on filtered $\delta^{15}N$ data (see SOM). The reason why we base our new gas chronology only on the $\delta^{15}N$ method is twofold. First the $\delta^{15}N$ method allows to produce a continuous gas age scale along TI, while the other two methods give only 3 tie points (at times when CH_4 varies abruptly: onset of Bølling, onset of Younger Dryas and onset of Holocene) and in particular cannot provide constraints for the onset of TI. Second, apart from the zero-convective zone assumption, the $\delta^{15}N$ method has the smallest analytical uncertainty (Figure 2).

The three approaches: $\delta^{15}N$, synchronization to EDML and TALDICE and seesaw methods

all disagree with the firn densification model simulation for EDC (Figure 2), which probably lacks important processes affecting densification under glacial conditions, such as the effect of increased impurities concentrations*16*.

A second step to examine the phasing between aCO_2 and AT during TI is to produce an accurate record of AT during the past (Antarctic Temperature Stack, ATS). To this aim, we stack (see SOM) the isotopic temperature reconstructions from 5 different ice cores (EDC, Vostok, Dome Fuji, TALDICE and EDML) after the synchronization of these ice cores onto the EDC one. This stacking process considerably reduces the noise in comparison to the individual EDC record (Figure 4): the standard deviation of ATS to its 220 yr moving average is 0.20°C while it is 0.52°C for the EDC temperature record (both ATS and the EDC temperature record being resampled every 20 yr).

The temporal variations of aCO_2 and AT across Termination I (Figure 4) on our chronology are highly correlated (Pearson correlation coefficient of 0.993 for 20 yr resampled time series). Both records can be accurately fitted by a 6 points linear function (Figure 4 and SOM). We infer the aCO_2-AT phasing at the 4 break points using a Monte-Carlo algorithm (see SOM): onset of TI (10±160 yr, 1σ, aCO_2 leads), onset of Bølling (-260±130 yr, AT leads), onset of Younger Dryas (60±120, aCO_2 leads) and onset of Holocene (-500±90, AT leads). The uncertainty takes into account the uncertainty in the break points determination and the uncertainty in the Δdepth determination. The only significant aCO_2-AT lags are observed at the onsets of the Bølling and the Holocene. It should be noted that during these two events, the associated sharp increases in aCO_2 were likely larger and more abrupt than the signals recorded in the ice core, due to the diffusion in the gas recording process*17*. This atmosphere-ice core difference biases our break point determination toward younger ages. If we use these fast increases to determine the break points in aCO_2, we find a lag of -10±130 yr (1σ) for the Bølling onset and -130±90 yr (1σ) for the Holocene onset, that is, no significant phasing. If, instead of using aCO_2, we use the radiative forcing of aCO_2*18* (rCO_2=5.35 W/m^2 ln(CO_2/280 ppmv), the inferred phasing is not significantly modified (Figure 4).

Our evaluation of the aCO_2 – AT phasing for TI differs from the 800±200 yr (lead of AT) estimate for Termination III*19*, based on the hypothesis that δ^{40}Ar of air is a gas proxy for local temperature. We cannot exclude the possibility that the aCO_2-AT phasing is different for TI and TIII. However, if as recently suggested*16* the LID is influenced by the impurity content of the firn, δ^{40}Ar, which, as δ^{15}N, follows a gravitational enrichment, should be paced by changes in dust concentration. We note that, during TIII, the change in dust occurs earlier than the change in ice isotope at both EDC and Vostok (see Figs. S7 and S8), while these two records are approximately in phase during TI (Fig. S8). This could explain why the Vostok δ^{40}Ar record is in advance with respect to the aCO_2 record, without contradicting our finding of synchronous changes in aCO_2 and AT. During TII at EDC (Fig. S8), on the other hand, the change in δ^{15}N occurs at a deeper depth than the change in dust. Dust concentration can therefore not be the only factor influencing the LID.

Our results are also in general agreement with a recent 0-400 yr aCO_2-AT average lag estimate for TI*20*, using a different approach. While this study does not make any assumption on the convective zone thickness, it is based on 1) coastal cores which might be

biased by local changes in ice sheet thickness and 2) firn densification models which may not be valid for past conditions (see SOM for a more detailed discussion).
Our chronology and the resulting aCO_2/AT phasing strengthens the hypothesis of a close coupling between aCO_2 and AT on both orbital and millennial time scales. The aCO_2 rise could contribute to much of the Antarctic temperature change during TI, even at its onset, accounting for positive feedbacks and polar amplification*21* which magnify the impact of the relatively weak rCO_2 change (Figure 4), that alone accounts for ~0.6°C of global warming during TI*21*. Invoking changes in the strength of the Atlantic meridional overturning circulation is no more required to explain the lead of AT over aCO_2*22*.
Given the importance of Southern Ocean in carbon cycle processes*23*, one should not exclude the possibility that aCO_2 and AT are interconnected through another common mechanism such as a relationship between sea ice cover and ocean stratification. While the tight link between aCO_2 and AT suggests a major common mechanism, reviews of carbon cycle processes suggest a complex association of numerous independent mechanisms*2, 23*.
In conclusion, changes of aCO_2 and AT were synchronous during TI within uncertainties. Our method, based on air ^{15}N measurements to determine the ice/gas depth shift, is currently used in the building of a new common and optimized chronology for all Antarctic ice cores*24, 25*. The assumption that no convective zone existed at EDC during TI might be tested in the future by using Krypton and Xenon isotopes*26.* Further studies on the firn are needed to understand the causes of the past variations of the LID, such as the possible impact of impurity concentrations on the densification velocity. While our study was focused on the *relative* timing of TI climatic records extracted from Antarctic ice cores, there is now the need to build a global chronological framework for greenhouse gases, temperature reconstructions and other climate proxies at various locations*22*. While the timings of the Bølling, Younger Dryas and Holocene onsets as visible in the methane records are now well constrained by a layer-counted Greenland chronology*27*, the timing of the onset of TI in Antarctic records remains challenging. Modeling studies using coupled carbon cycle/climate models will be needed to fully explore the implications of this synchronous change of AT and aCO_2 during TI for our understanding of natural climate changes mechanisms.

References

1. Monnin, E., Indermühle, A., Dällenbach, A., Flückiger, J., Stauffer, B., Stocker, T.F., Raynaud, D., and Barnola, J.-M. Atmospheric CO_2 concentrations over the last glacial termination. *Science* **291**, p. 112-114 (2001).
2. Lourantou, A., Lavric;, J.V., Köhler, P., Barnola, J.-M., Paillard, D., Michel, E., Raynaud, D., and Chappellaz, J. Constraint of the CO_2 rise by new atmospheric carbon isotopic measurements during the last deglaciation. *Global Biogeochem. Cycles* **24**, p. GB2015 (2010).
3. Fischer, H., Wahlen, M., Smith, J., Mastroianni, D., and Deck, B. Ice Core Records of Atmospheric CO_2 Around the Last Three Glacial Terminations. *Science* **283**, p. 1712-1714 (1999).
4. Loulergue, L., Parrenin, F., Blunier, T., Barnola, J.-M., Spahni, R., Schilt, A., Raisbeck, G., and Chappellaz, J. New constraints on the gas age-ice age difference along the EPICA ice cores, 0-50 kyr. *Clim. Past* **3**, p. 527-540 (2007).
5. Parrenin, F., Barker, S., Blunier, T., Chappellaz, J., Jouzel, J., Landais, A., Masson-Delmotte, V., Schwander, J., and Veres, D. On the gas-ice depth difference (Δdepth) along the EPICA Dome C ice core. *Clim. Past* **8**, p. 1239-1255 (2012).
6. Goujon, C., Barnola, J.-M., and Ritz, C. Modeling the densification of polar firn including heat diffusion: application to close-off characteristics and gas isotopic fractionation for Antarctica and Greenland sites. *J. Geophys. Res.* **108**, p. ACL10/1-10 (2003).
7. Parrenin, F., Dreyfus, G., Durand, G., Fujita, S., Gagliardini, O., Gillet, F., Jouzel, J., Kawamura, K., Lhomme, N., Masson-Delmotte, V., Ritz, C., Schwander, J., Shoji, H., Uemura, R., Watanabe, O., and Yoshida, N. Ice flow modelling at EPICA Dome C and Dome Fuji, East Antarctica. *Clim. Past* **3**, p. 243-259 (2007).
8. Craig, H., Horibe, Y., and Sowers, T. Gravitational Separation of Gases and Isotopes in Polar Ice Caps. *Science* **242**, p. 1675-1678 (1988).
9. Sowers, T.A., Bender, M., Raynaud, D., and Korotkevich, Y.L. The $\delta^{15}N$ of N_2 in air trapped in polar ice : a tracer of gas transport in the firn and a possible constraint on ice age-gas age differences. *J. Geophys. Res.* **97**, p. 15683-15697 (1992).
10. Landais, A., Barnola, J., Kawamura, K., Caillon, N., Delmotte, M., Ommen, T.V., Dreyfus, G., Jouzel, J., Masson-Delmotte, V., Minster, B., Freitag, J., Leuenberger, M., Schwander, J., Huber, C., Etheridge, D., and Morgan, V. Firn-air $\delta^{15}N$ in modern polar sites and glacial-interglacial ice: a model-data mismatch during glacial periods in Antarctica?. *Quat. Sci. Rev.* **25**, p. 49-62 (2006).
11. Dreyfus, G.B., Jouzel, J., Bender, M.L., Landais, A., Masson-Delmotte, V., and Leuenberger, M. Firn processes and $\delta^{15}N$: potential for a gas-phase climate proxy. *Quat. Sci. Rev.* **29**, p. 28-42 (2010).
12. Severinghaus, J.P., Albert, M.R., Courville, Z.R., Fahnestock, M.A., Kawamura, K., Montzka, S.A., Mühle, J., Scambos, T.A., Shields, E., Shuman, C.A., Suwa, M., Tans, P., and Weiss, R.F. Deep air convection in the firn at a zero-accumulation site, central

Antarctica. *Earth Planet. Sci. Lett.* **293**, p. 359-367 (2010).
13. Stocker, T.F., and Johnsen, S.J. A minimum thermodynamic model for the bipolar seesaw. *Paleoceanography* **18**, p. 1-9 (2003).
14. Raisbeck, G.M., Yiou, F., Jouzel, J., and Stocker, T.F. Direct north-south synchronization of abrupt climate change record in ice cores using Beryllium 10. *Clim. Past* **3**, p. 541-547 (2007).
15. Barker, S., Knorr, G., Edwards, R.L., Parrenin, F., Putnam, A.E., Skinner, L.C., Wolff, E., and Ziegler, M. 800,000 Years of Abrupt Climate Variability. *Science* **334**, p. 347-351 (2011).
16. Hörhold, M., Laepple, T., Freitag, J., Bigler, M., Fischer, H., and Kipfstuhl, S. On the impact of impurities on the densification of polar firn. *Earth Planet. Sci. Lett.* **325–326**, p. 93-99 (2012).
17. Köhler, P., Knorr, G., Buiron, D., Lourantou, A., and Chappellaz, J. Abrupt rise in atmospheric CO_2 at the onset of the Bølling/Allerød: in-situ ice core data versus true atmospheric signals. *Clim. Past* **7**, p. 473-486 (2011).
18. Myhre, G., Highwood, E.J., Shine, K.P., and Stordal, F. New estimates of radiative forcing due to well mixed greenhouse gases. *Geophys. Res. Lett.* **25**, p. 2715-2718 (1998).
19. Caillon, N., Severinghaus, J.P., Jouzel, J., Barnola, J.-M., Kang, J., and Lipenkov, V.Y. Timing of Atmospheric CO_2 and Antarctic Temperature Changes Across Termination III. *Science* **299**, p. 1728-1731 (2003).
20. Pedro, J.B., Rasmussen, S.O., and van Ommen, T.D. Tightened constraints on the time-lag between Antarctic temperature and CO$_2$ during the last deglaciation. *Clim. Past* **8**, p. 1213-1221 (2012).
21. Köhler, P., Bintanja, R., Fischer, H., Joos, F., Knutti, R., Lohmann, G., and Masson-Delmotte, V. What caused Earth's temperature variations during the last 800,000 years? Data-based evidence on radiative forcing and constraints on climate sensitivity. *Quat. Sci. Rev.* **29**, p. 129 - 145 (2010).
22. Shakun, J.D., Clark, P.U., He, F., Marcott, S.A., Mix, A.C., Liu, Z., Otto-Bliesner, B., Schmittner, A., and Bard, E. Global warming preceded by increasing carbon dioxide concentrations during the last deglaciation. *Nature* **484**, p. 49-54 (2012).
23. Fischer, H., Schmitt, J., Lüthi, D., Stocker, T.F., Tschumi, T., Parekh, P., Joos, F., Köhler, P., Völker, C., Gersonde, R., Barbante, C., Floch, M.L., Raynaud, D., and Wolff, E. The role of Southern Ocean processes in orbital and millennial CO_2 variations – A synthesis. *Quat. Sci. Rev.* **29**, p. 193-205 (2010).
24. Bazin, L., Landais, A., Lemieux-–Dudon, B., Kele, H.T.M., Veres, D., Parrenin, F., Martinerie, P., Ritz, C., Capron, E., Lipenkov, V., Loutre, M.-F., Raynaud, D., Vinther, B., Svensson, A., Rasmussen, S., Severi, M., Blunier, T., Leuenberger, M., Fischer, H., Masson-–Delmotte, V., Chappellaz, J., and Wolff, E. An optimized multi-proxies, multi-site Antarctic ice and gas orbital chronology (AICC2012). *Climate of the Past, submitted* (2012).
25. Veres, D., Bazin, L., Landais, A., Lemieux-Dudon, B., Parrenin, F., Martinerie, P., Toyé Mahamadou Kele, H., Capron, E., Chappellaz, J., Rasmussen, S., Severi, M.,

Svensson, A., Vinther, B., and Wolff, E. The Antarctic ice core chronology (AICC2012): an optimized multi-parameter and multi-site dating approach for the last 120-thousand years. *Climate of the Past, submitted* (2012).
26. Severinghaus, J.P., Grachev, A., Luz, B., and Caillon, N. A method for precise measurement of argon 40/36 and krypton/argon ratios in trapped air in polar ice with applications to past firn thickness and abrupt climate change in Greenland and at Siple Dome, Antarctica. *Geochim. Cosmochim. Acta* **67**, p. 325 - 343 (2003).
27. Svensson, A., Andersen, K.K., Bigler, M., Clausen, H.B., Dahl-Jensen, D., Davies, S.M., Johnsen, S.J., Muscheler, R., Parrenin, F., Rasmussen, S.O., Röthlisberger, R., Seierstad, I., Steffensen, J.P., and Vinther, B.M. A 60 000 year Greenland stratigraphic ice core chronology. *Clim. Past* **4**, p. 47-57 (2008).
28. Jouzel, J., Masson-Delmotte, V., Cattani, O., Dreyfus, G., Falourd, S., Hoffmann, G., Minster, B., Nouet, J., Barnola, J.M., Chappellaz, J., Fischer, H., Gallet, J.C., Johnsen, S., Leuenberger, M., Loulergue, L., Luethi, D., Oerter, H., Parrenin, F., Raisbeck, G., Raynaud, D., Schilt, A., Schwander, J., Selmo, E., Souchez, R., Spahni, R., Stauffer, B., Steffensen, J.P., Stenni, B., Stocker, T.F., Tison, J.L., Werner, M., and Wolff, E.W. Orbital and Millennial Antarctic Climate Variability over the Past 800,000 Years. *Science* **317**, p. 793-796 (2007).
29. Loulergue, L., Schilt, A., Spahni, R., Masson-Delmotte, V., Blunier, T., Lemieux, B., Barnola, J.M., Raynaud, D., Stocker, T.F., and Chappellaz, J. Orbital and millennial-scale features of atmospheric CH_4 over the past 800,000 years. *Nature* **453**, p. 383-386 (2008).

Ackowledgements: We thank O. Watanabe, B. Stenni and EPICA community members for giving access to respectively the DF1, TALDICE and EDML isotopic data. We thank L. Loulergue, D. Buiron and T. Blunier for giving access to respectively the EDC-EDML, TALDICE and GRIP CH_4 data. We thank G. Dreyfus for giving access to the $\delta^{15}N$ isotopic data. We thank G. Delaygue, J. Chappellaz, S. Barker and A. Ganopolski for helpful discussions. This work greatly benefited from constructive comments by the editor J. Smith and by two anonymous reviewers. This work is a contribution to the European Project for Ice Coring in Antarctica (EPICA), a joint European Science Foundation/European Commission scientific program, funded by the EU and by national contributions from Belgium, Denmark, France, Germany, Italy, the Netherlands, Norway, Sweden, Switzerland and the United Kingdom. The main logistic support was provided by IPEV and PNRA at Dome C. We thank the technical teams in the field and at the different laboratories. This is EPICA publication n°xx.

Fig. 1. Scheme illustrating the deduction of the Δdepth at EDC from ice (volcanic) and gas (CH_4) synchronization to the EDML or TADLICE ice cores and evaluation of Δdepth at EDML or TALDICE.

Fig. 2. Estimation of the Δdepth along the EDC ice core using different methods: purely based on modeling (densification and ice flow, grey line), based on $\delta^{15}N$ data and ice flow modeling (orange dots), based on the synchronization to the EDML ice core (blue square), based on the synchronization to the TALDICE ice core (green square), based on the bipolar seesaw hypothesis (red triangle). The black line is a fit (see SOM) to the $\delta^{15}N$ estimates and the dashed lines represent its 1σ confidence interval. 1σ uncertainties estimation is described in*5* and in the SOM.

Fig. 3. The bipolar seesaw hypothesis allows to derive 3 Δdepth estimates at EDC during the last deglacial warming using the 100-yr resampled δD record*28* and the CH_4 record*29*. Error bars on depths of tie points are 1σ. EDC gas depth scale is linearly stretched according to the tie points.

Fig. 4. Various climate time series during TI. δD from EDC*28* (purple), ATS (blue, this study) and confidence interval (light blue), aCO_2 from EDC*1, 2* (light green), rCO_2 (dark green), atmospheric CH_4 from EDC*29* (red) and Greenland $\delta^{18}O$ from NorthGRIP onto the GICC05 age scale*27* with a 220 yr running average (dark grey). The solid lines represent the best 6 points linear fit of ATS, aCO_2 and rCO_2 (see SI). The vertical dashed lines mark the 4 break points in ATS (blue) and in aCO_2 (green), where we evaluate the aCO_2-AT and the rCO_2-AT phase lags (black numbers). The new EDC age scale is described in the SOM.

Supplementary Materials:

Materials and Methods

Supplementary Text

Figs. S1 to S8

Tables S1 to S7

Database S1

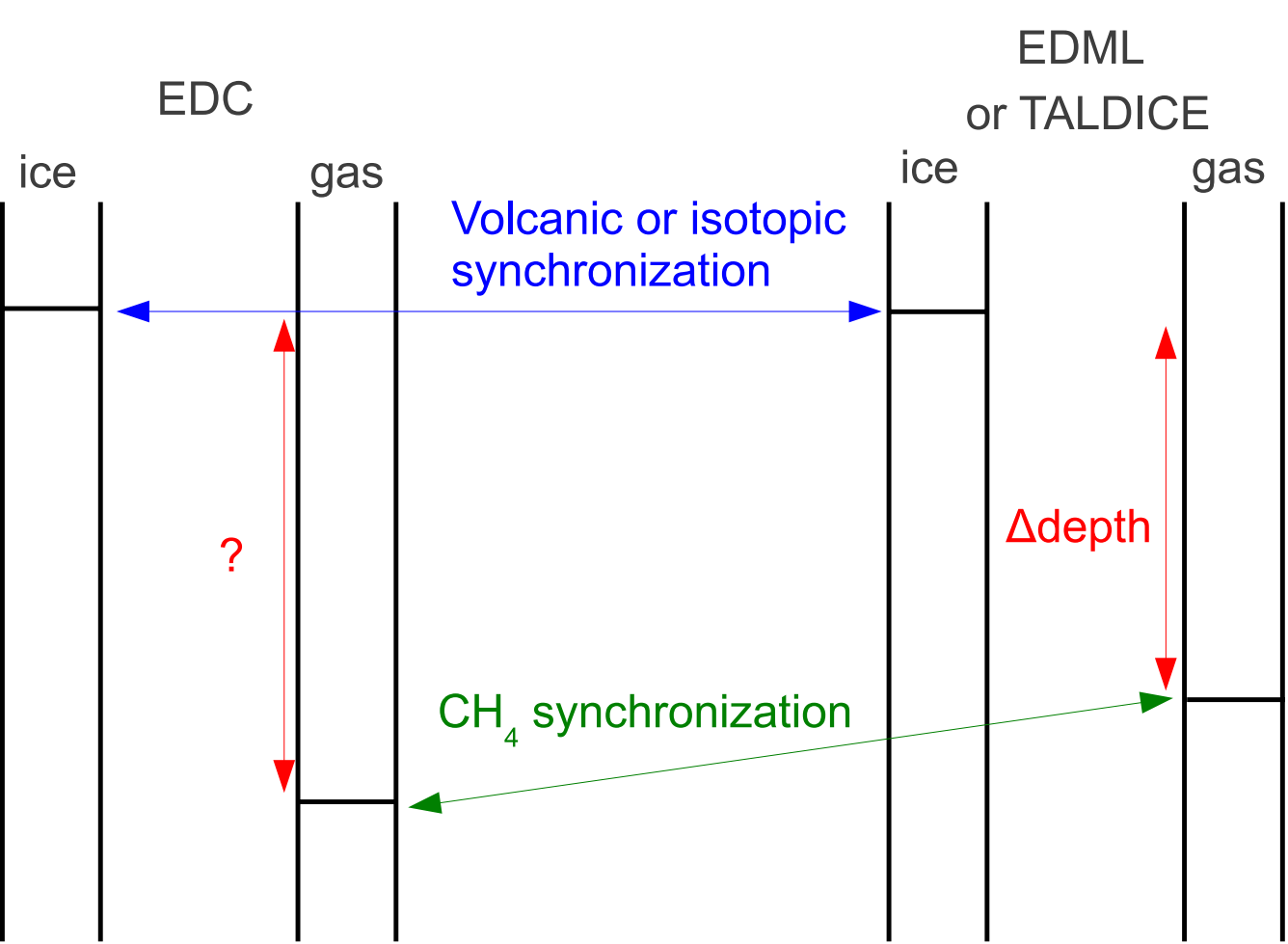
EDC
EDML
or TALDICE
ice
gas
ice
gas
Volcanic or isotopic
synchronization
?
Δdepth
CH4 synchronization

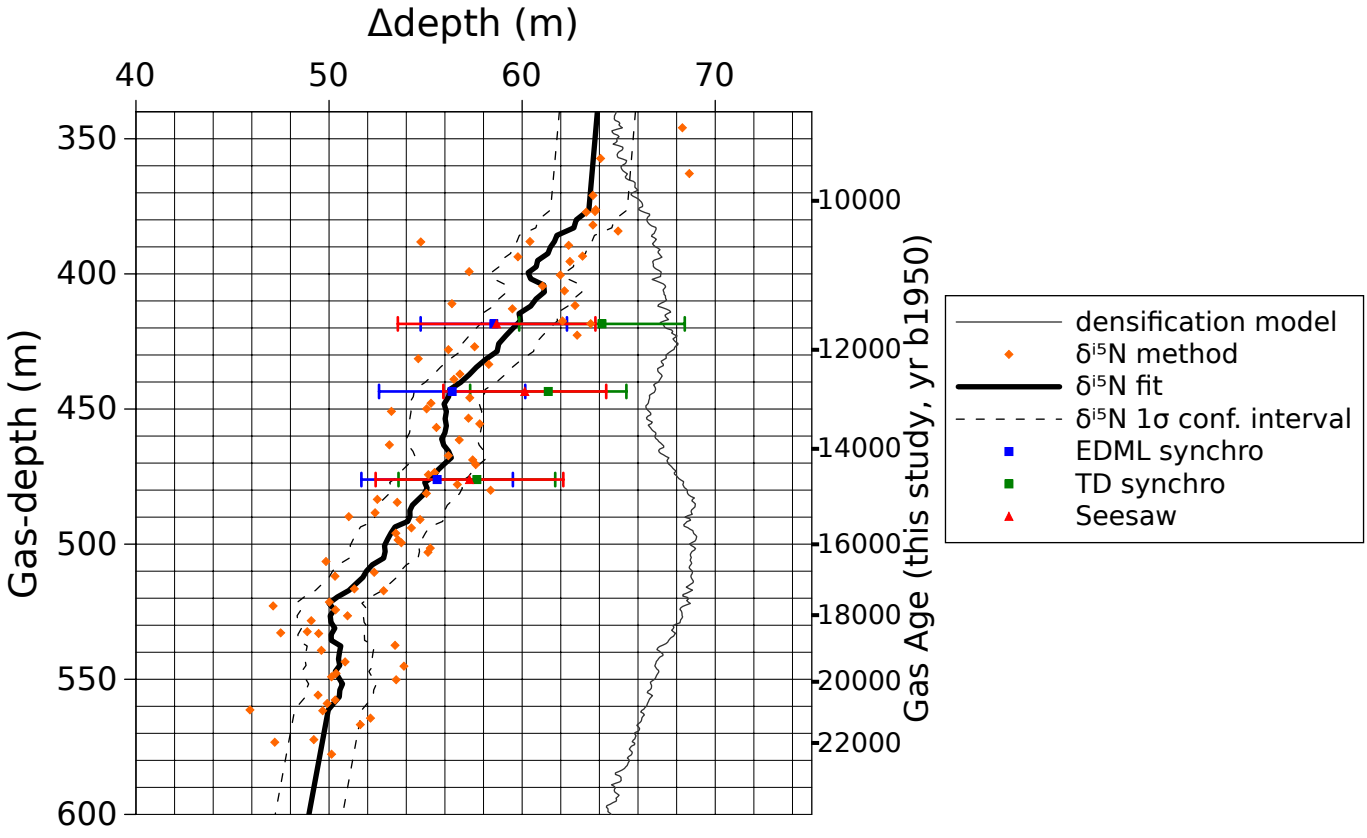
Δdepth (m)
40
50
60
70
Gas-depth (m)
350
400
450
500
550
600
Gas Age (this study, yr b1950)
10000
12000
14000
16000
18000
20000
22000
densification model
δ¹⁵N method
δ¹⁵N fit
δ¹⁵N 1σ conf. interval
EDML synchro
TD synchro
Seesaw

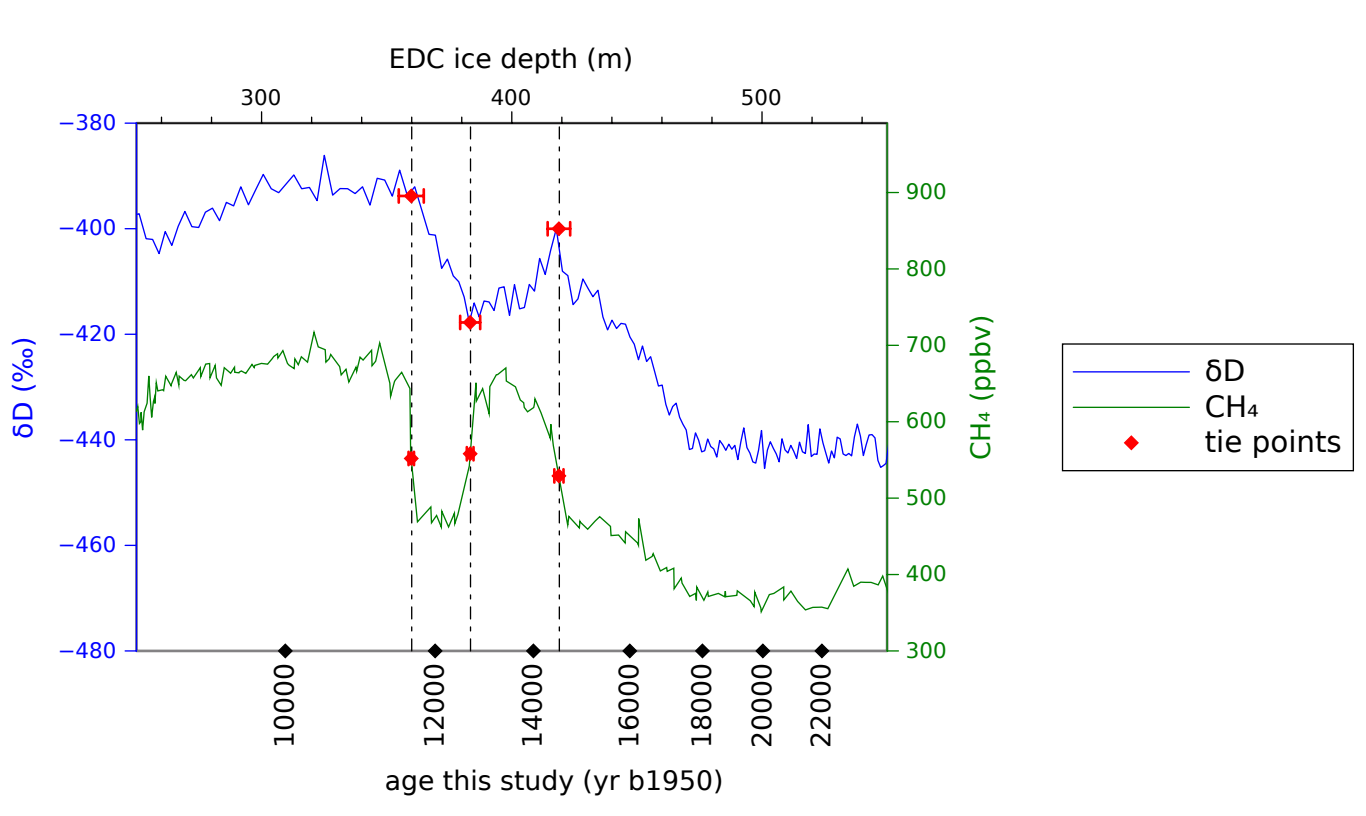
EDC ice depth (m)
300
400
500
−380
−400
−420
−440
−460
−480
δD (‰)
900
800
700
600
500
400
300
CH₄ (ppbv)
δD
CH₄
tie points
10000
12000
14000
16000
18000
20000
22000
age this study (yr b1950)

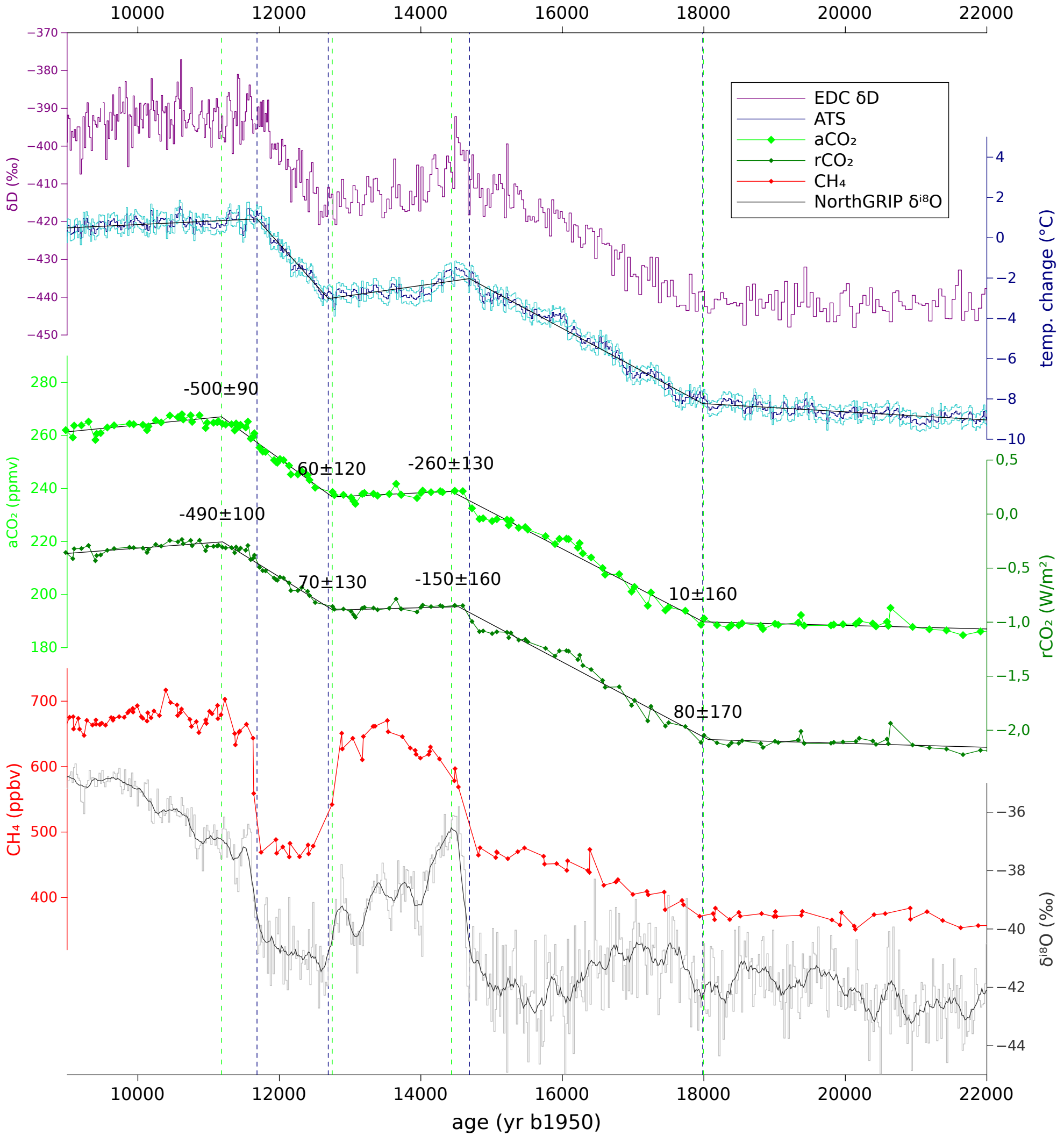
10000
12000
14000
16000
18000
20000
22000
δD (‰)
−370
−380
−390
−400
−410
−420
−430
−440
−450
EDC δD
ATS
aCO₂
rCO₂
CH₄
NorthGRIP δ¹⁸O
temp. change (°C)
4
2
0
−2
−4
−6
−8
−10
aCO₂ (ppmv)
280
260
240
220
200
180
-500±90
60±120
-260±130
-490±100
70±130
-150±160
10±160
80±170
rCO₂ (W/m²)
0,5
0,0
−0,5
−1,0
−1,5
−2,0
CH₄ (ppbv)
700
600
500
400
δ¹⁸O (‰)
−36
−38
−40
−42
−44
age (yr b1950)

Supplementary Materials for

Synchronous change of atmospheric CO_2 and Antarctic temperature during the last deglacial warming

F. Parrenin, V. Masson-Delmotte, P. Köhler, D. Raynaud, D. Paillard, J. Schwander, C. Barbante, A. Landais, A. Wegner and J. Jouzel

correspondence to: parrenin@ujf-grenoble.fr

This PDF file includes:

Materials and Methods
Supplementary Text
Figs. S1 to S8
Tables S1 to S7

Other Suplementary Materials for this manuscript includes the following:

Database S1

Materials and Methods

Estimating Δdepth from air $\delta^{15}N$ data

The principles of using air $\delta^{15}N$ data to estimate Δdepth have been described elsewhere *(1)*. It is not possible to directly use the raw $\delta^{15}N$-based Δdepth estimates because they are noisy. As a proof, the $\partial\Delta depth/\partial z$ function estimated from these raw data (1) sometimes exceeds 1, which would mean that the gas layers are inverted. The reason is probably the ice quality, since 1) the ice is brittle at these depths; 2) the pooled standard deviation of the measurements is only <0.012‰ *(2)*, equivalent to ~2 m of LID and is not significantly higher for the last deglaciation than for older time periods. We therefore apply a 13 points moving average fit (Fig. 1). The fit is extrapolated in the 340-376.35 m and 561.31-600 m intervals by assuming the LID in ice equivalent is constant and only the variations of ice thinning impact Δdepth. We inferred that 13 was the optimal number of points for the running average by studying the residuals: using less points results in anti-correlated residuals while using more points results in correlated residuals. By doing this smoothing, we assume that on average, the $\delta^{15}N$ data are representative of the $\delta^{15}N$ content of the air at the bottom of the diffusive zone. This is corroborated by the quasi-symetrical distribution of the residuals (2). Based on the standard deviation of the distance of the $\delta^{15}N$-based Δdepth estimates to the fit (linearly interpolated in depths), we estimate their 1σ accuracy to be ~2 m, which translates into a 0.6 m 1σ accuracy for the fit. We neglect the error in the linear interpolation in depths procedure because the average sampling is only ~2.4 m. We also added 1σ uncertainties of 1% due to the dependence of the gravitational enrichment to the poorly known temperature during the past *(1)*, 0.5% due to the poorly known temperature gradient in the firn *(1)* and 2.5% due to the poorly known average firn relative density *(1)*. Another source of uncertainty is due to the thinning function evaluation. It has been evaluated to range between 1% and 1.8% in the 340-600 m depth interval considered here *(1)*.

In our study we have assume that the past convective zone thickness was negligible. One potential cause for variations in this physical variable is the change in surface winds. GCM experiments for the LGM shows little variations in wind on the East Antarctic plateau *(3)*.

Construction of the age scale

Our ice age scale is a modified version of the EDC3 ice age scale *(4)*. We first corrected for a depth offset between the EDC96 and EDC99 ice cores and added 55 yr to the EDC3 age scale for ages older than 45.6 kyr. We then computed gas ages from this $EDC3_{corr}$ ice age scale for the EDC CH_4 record *(5)* based on our $\delta^{15}N$-based Δdepth estimates. We found that this new gas age scale does not perfectly fit with the GICC05 age scale *(6)* by comparing the CH_4 transitions *(7)*. We therefore decided to modify the $EDC3_{corr}$ ice age scale in the interval between 5280 yr b1950 (where there exists an absolute tie point derived from the comparison between Antarctic ^{10}Be and ^{14}C from the dendrochronology)

and 41,200 yr b1950 (^{10}Be peak corresponding to the Laschamp geomagnetic event). We therefore linearly interpolated the $EDC3_{corr}$ ice age scale according to the tie points listed in Table S1 to get a perfect fit with ages ties (see 3 for the resulting CH_4 synchronization to GRIP/GICC05). This ice age scale has however negligible impact on the discussion of the aCO_2-AT phasing, which mainly depends on the Δdepth estimates.

An Antarctic temperature stack, 0-800 kyr b1950

Here we produce a stack of Antarctic temperature variations during the past 800 kyr, based on available ice core data (2) at EPICA Dome C (EDC), Dome Fuji (DF), Vostok, Talos Dome (TALDICE) and EPICA Dronning Maud land (EMDL). A preliminary work is the synchronization of all the DF, Vostok, TALDICE and EDML ice cores to the EDC one, based on volcanic matching, where available and isotopic matching elsewhere (using the break points). The isotopic records at each site are converted to temperature records using the classical isotopic thermometer, with correction for $\delta^{18}O$ variations in the ocean caused by land ice variations. The stack is then simply constructed, for each time in the past, as the average of all available ice core temperature records.

Ice isotope variations recorded in ice cores are corrected for ocean sea water (SW) isotope variations following the approach by Stenni et al. *(8)*:

$$\delta^{18}O_{corr} = \delta^{18}O_{ice} - \delta^{18}O_{sw} \times \frac{1+\delta^{18}O_{ice}/1000}{1+\delta^{18}O_{sw}/1000} \quad (1)$$

$$\delta D_{corr} = \delta D_{ice} - 8\delta^{18}O_{sw} \times \frac{1+\delta D_{ice}/1000}{1+8\delta^{18}O_{sw}/1000} \quad (2)$$

$\delta^{18}O_{sw}$ has been inferred *(9)* based on an ocean isotopic stack *(10)*. We put the $\delta^{18}O_{sw}$ record on the EDC3 age scale by synchronizing the polar temperature reconstruction *(9)* with the EDC isotopic record (see Table 6).

The temperature at each ice core site is then simply evaluated as:

$$\Delta T_{clim} = 1/\alpha \times \Delta\delta D_{corr} \quad (3)$$

or

$$\Delta T_{clim} = 8/\alpha \times \Delta\delta^{18}O_{corr} \quad (4)$$

with α=6.04 ‰/°C *(11)*. First, we shift the EDC temperature reconstruction to obtain an average ΔT_{clim}=0 over the time interval 0-1 kyr b1950 is 0. Second, we rescaled the temperature reconstruction from each ice core so that the resulting ΔT_{clim} has the same average and standard deviation than the EDC one on the interval 0-140 kyr b1950, where all ice cores temperature reconstructions are available.

The EDC3 chronology *(4)* is transferred onto each ice cores using the tie points described above. Each temperature record is then resampled using an averaging over 20 yr intervals. For each of these 20 yr long time interval, the average of all available ice core temperature reconstructions is computed. The stack is again further scaled to have a 0

average over the time interval 0-1 kyr b1950. A pooled standard deviation is calculated for the stack, as:

$$\sigma_{\text{pooled}} = \left(\frac{\sum_{i,j=1}^{n,m} (T_i - \bar{T}_j)^2}{n-m} \right)^{1/2} , \quad (5)$$

which is the root of the sum of the squared differences of the individual temperature reconstructions T_i from the stack T_j divided by the degree of freedom, in this case the number of individual temperature values n minus the number of stacked temperature values m. For each age, the confidence interval of the stack is simply evaluated as:

$$\sigma = \frac{\sigma_{\text{pooled}}}{\sqrt{N}} , \quad (6)$$

where N is the number of isotopic records.

Fit of AT, aCO_2 and rCO_2 by *6* points linear functions

We search for the 6 points continuous and linear by interval functions (Figure S5) which best fit the AT, aCO_2 and rCO_2 records defined by N data points (t_i,y_i). We define the density of probability of such a fit $y(t)$ defined by its 6 points (T_i,Y_i), i=0,...,5 (we fix T_0=9000 yr and T_5=22000 yr the boundaries of our time interval), by:

$$P = k \cdot \exp\left(-\sum_{i=0}^{N} \frac{(y(t_i) - y_i)^2}{\sigma^2} \right) , \quad (7)$$

where k is a multiplicative constant, σ is an uncertainty which includes both the uncertainty on the data value y_i and the uncertainty of the 6 points linear model *(12)*. In practice, σ is evaluated as the standard deviation of the residuals of the data value y_i to a first best 6 points linear function (6). By writing Equation (7), we implicitly assume that those uncertainties for each data point y_i are independent. In such a case, the modeling uncertainties are correlated at short time scales. Again by studying the residuals (6), we evaluated that there is no correlation for a distance between the t_i ≥200 yr for AT and ≥400 yr for aCO_2 and rCO_2. We thus resampled the AT, aCO_2 and rCO_2 records every 200 yr, 400 yr and 400 yr respectively. The evaluation of σ is consequently updated to 0.177 °C for AT, 1.22 ppmv for aCO_2 and 0.0333 W/m^2 for rCO_2. Our resampling approach is conservative and probably overestimates the real confidence intervals.

The densities of probabilities of T_i, i=1,...,4 and Y_i, i=0,...,5 are reconstructed by a Monte Carlo exploration based on the Metropolis-Hastings algorithm *(13, 14)*. Note that the algorithm only needs to evaluate the ratio of the densities of probability between two scenario, thus there is no need to know the multiplicative constant k. The Monte-Carlo sampling is composed of 10,000 scenarii, which ensure robust statistics. We use here the mean and the standard deviation of the probability distributions. The inferred values for T_i, i=1,...,4 and its confidence interval are given in 7.

Supplementary Text

Discussion of the ATS stack

There are three main sources of uncertainties on estimates of past AT changes based on water stable isotopes from deep ice cores:

- Changes in elevation at the coring site (mainly due to accumulation variations and isostasy *(15)*) which can produce glaciological artefacts. While attempts have been conducted to correct for elevation changes using glaciological models *(15-17)*, significant uncertainties remain *(18)*.

- In the cases of Vostok and EDML, upstream effects induced by ice flow such as elevation variations, which are not corrected for in this study *(18)*. These effects should be limited for TI.

- Changes in precipitation intermittency (and covariance between temperature and precipitation, at synoptic or seasonal scales). There is no mean to quantify such bias based on ice core data. While such bias has been simulated for climate projections *(19)* and suggested at the orbital scale *(20)*, several climate model simulations suggest that this bias may be limited for central Antarctica, between LGM and present day *(8, 16)*.

- Changes in moisture sources / evaporation conditions, affecting the initial water vapor isotopic composition. Information on past evaporation conditions (surface temperature, relative humidity) can be derived from deuterium excess and ^{17}O-excess. The combination of such data and isotopic distillation models allows to quantify the impact of changes in moisture sources on reconstructed Antarctic temperature. Deuterium excess studies are available for Vostok *(21)*, EDC and EDML *(8, 22)* and Dome F *(23, 24)*. Multiple ice core ^{17}O-excess studies have recently been published *(25)*. Despite significant methodological uncertainties *(24)*, these studies suggest limited moisture source impacts on temperature reconstructions for the last deglaciation.

The oceanic correction applied to our isotopic records contains only long-term fluctuations (typical period is 20 kyr, the precession period) and therefore is thought to not impact the detection of the break points in AT.

Here we did not use the Byrd, Siple Dome and Law Dome ice cores because their isotopic records do not resemble the common central East Antarctic scenario, and thus could be affected by local biases (such as larger changes of ice sheet elevation *(26)*). For example, the Byrd isotopic record shows an early warming at the onset of TI which is not in phase with the onset of TI in other Antarctic ice cores (a fluorine spike can be used to assess such phasing). The Siple Dome isotopic record shows a sharp isotopic event at ~22 kyr b1950 which has no counterpart in other ice cores. The Law Dome isotopic record does not show a stable temperature scenario during the early Holocene *(27)* which makes the estimate of the youngest break point very uncertain.

Moreover, we did not use methane synchronization in our stack because 1) it is only robust when methane varies abruptly and this is for example not the case at the onset of TI

and 2) it requires to estimate the past LID from firn densification models and even for high accumulation sites like EDML and TALDICE, these models could for some periods overestimate the LID by ~20% (28), leading to an ice age scale ~300 yr too old.

An alternative isotopic stack has already been constructed for TI *(29)*, using the records from Law Dome, Byrd, Siple Dome, EDML and TALDICE and based on methane synchronization. For the above mentioned reasons, we used here a different approach both for the synchronization of the ice cores and for the evaluation of the ice/gas shift. Both stacks are compared in Figure S4. The stack from *(29)* seems to be generally shifted by ~300 yr toward older ages with respect to our stack in the period from the onset of TI to the Antarctic Cold Reversal. This shift could be explained by either an overestimation of the modeled Δage or by local artefacts in the isotopic records of (29, 30), or by an underestimation of the convective zone thickness in our study, or by a combination of both.

Additional Data file S1 (separate file)

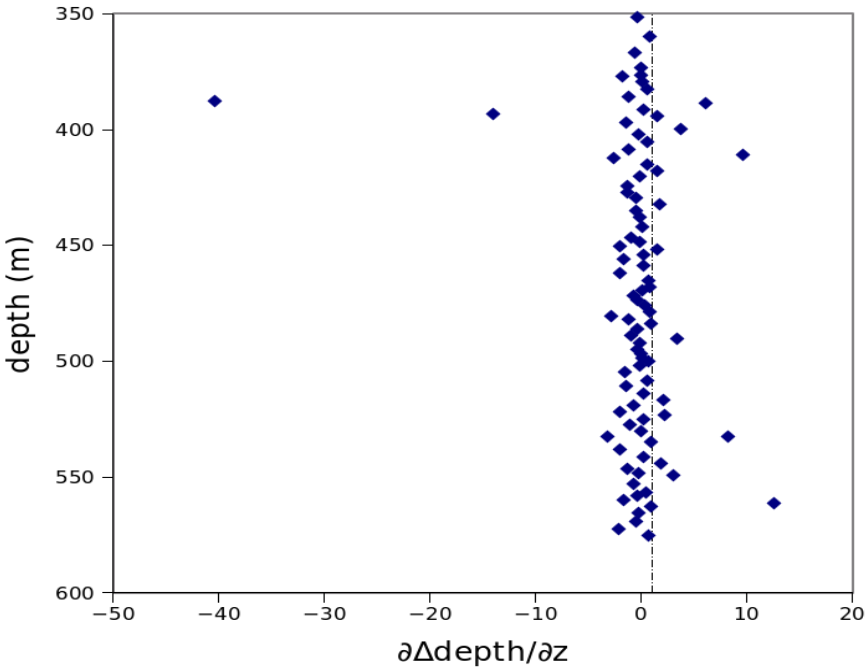

Fig. S1

∂Δdepth/∂z function as derived from the raw δ^{15}N-based Δdepth estimates. Vertical dashed line is for ∂Δdepth/∂z=1.

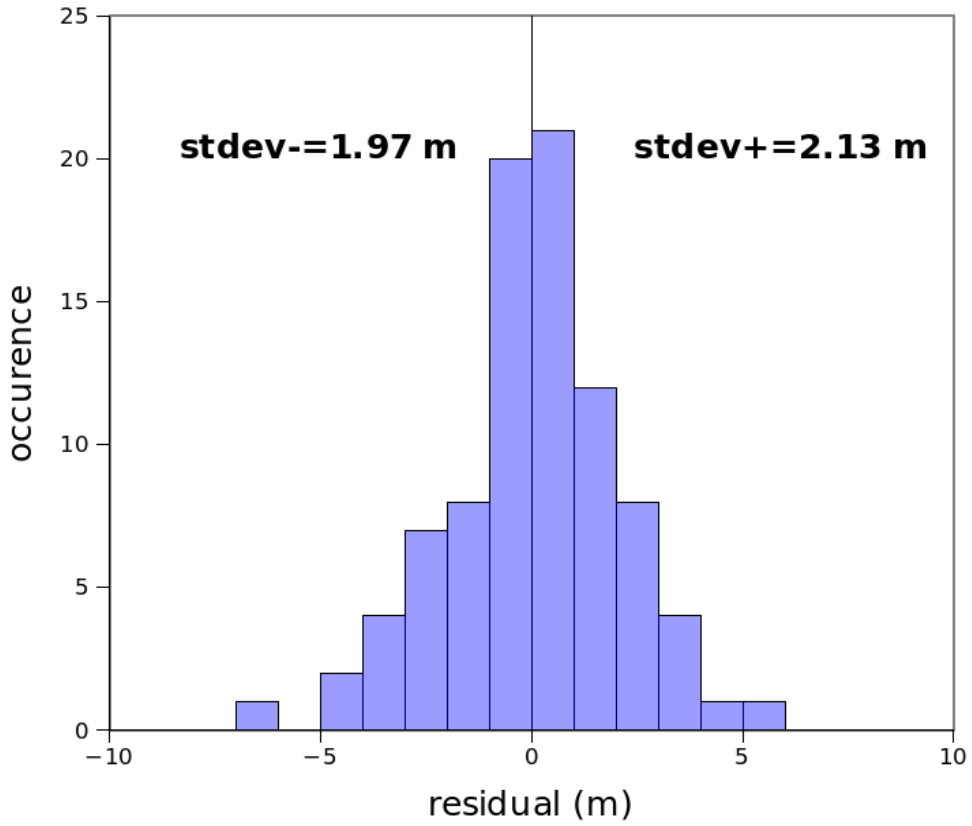

Fig. S2

Distribution of the residuals of $\delta^{15}N$-based Δdepth estimates to the fit. The standard deviation to zero of the positive and negative residuals is indicated.

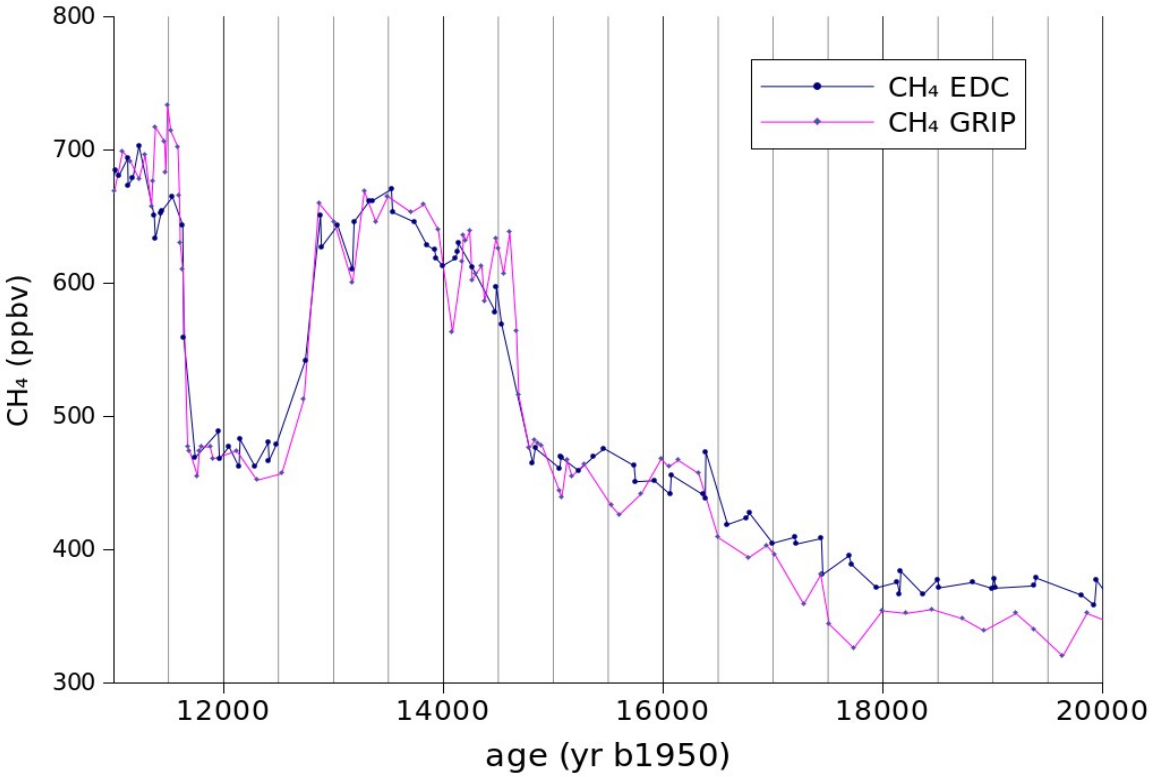

Fig. S3

Comparison between GRIP CH_4 record on the GICC05 age scale *(7)* with the EDC CH_4 record *(5)* on our age scale. GRIP CH_4 record is offset by -20 ppbv to take into account the interhemispheric CH_4 gradient during the 16-11 ka time interval.

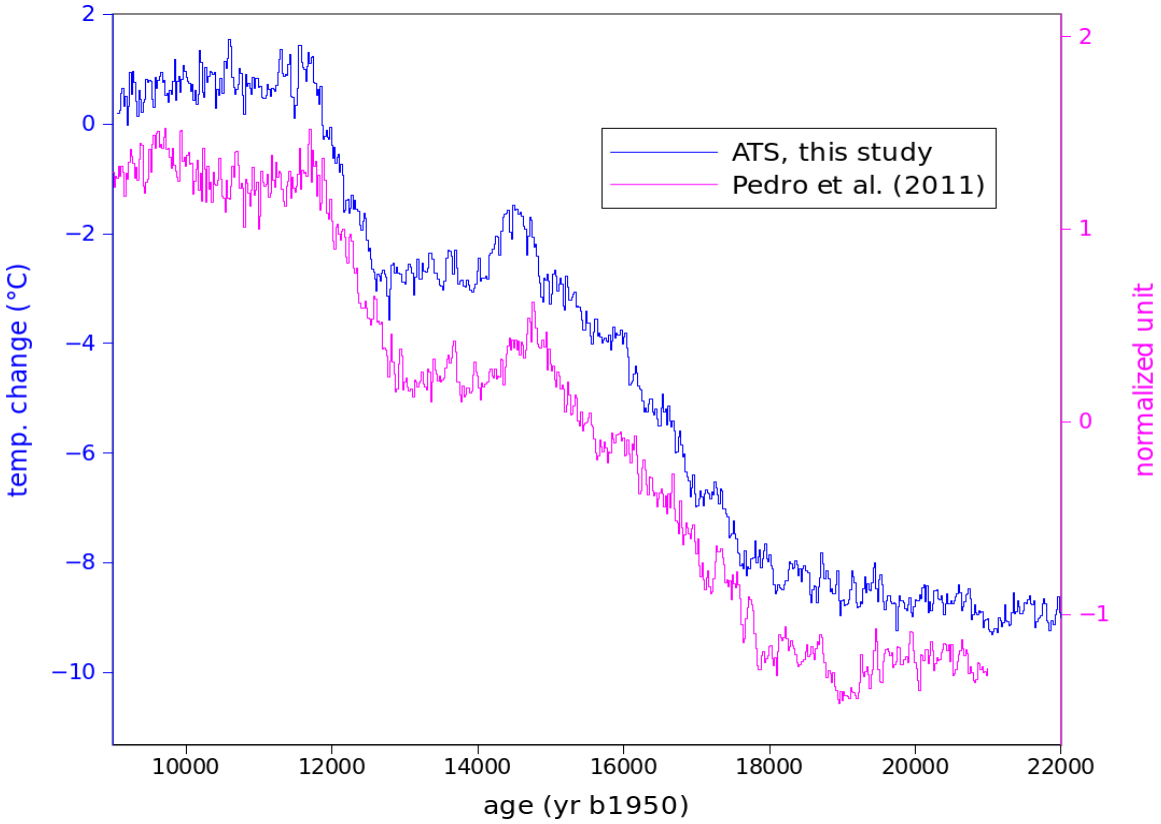

Fig. S4

Comparison of the ATS stack from this study with the Antarctic isotopic stack from (29).

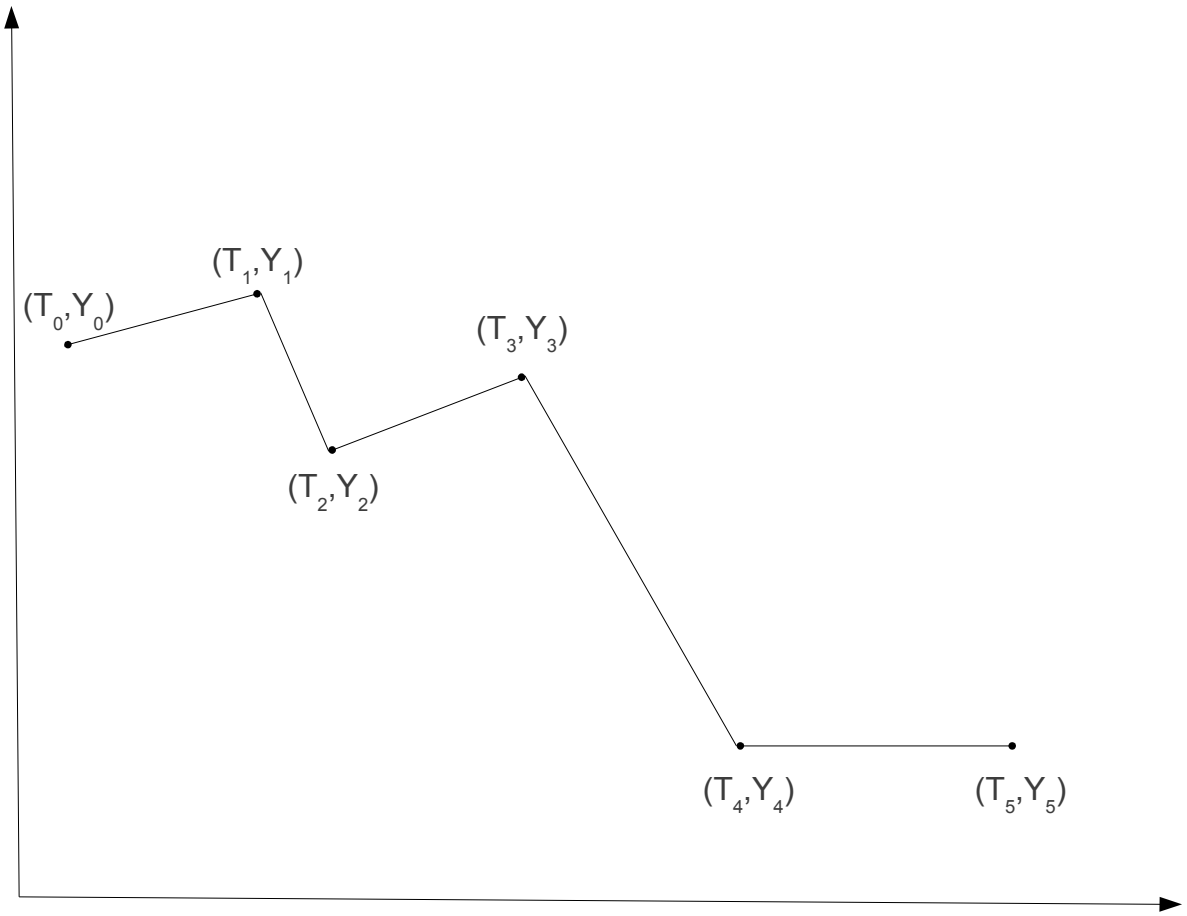

Fig. S5

Scheme illustrating a 6 points continuous and linear by interval function.

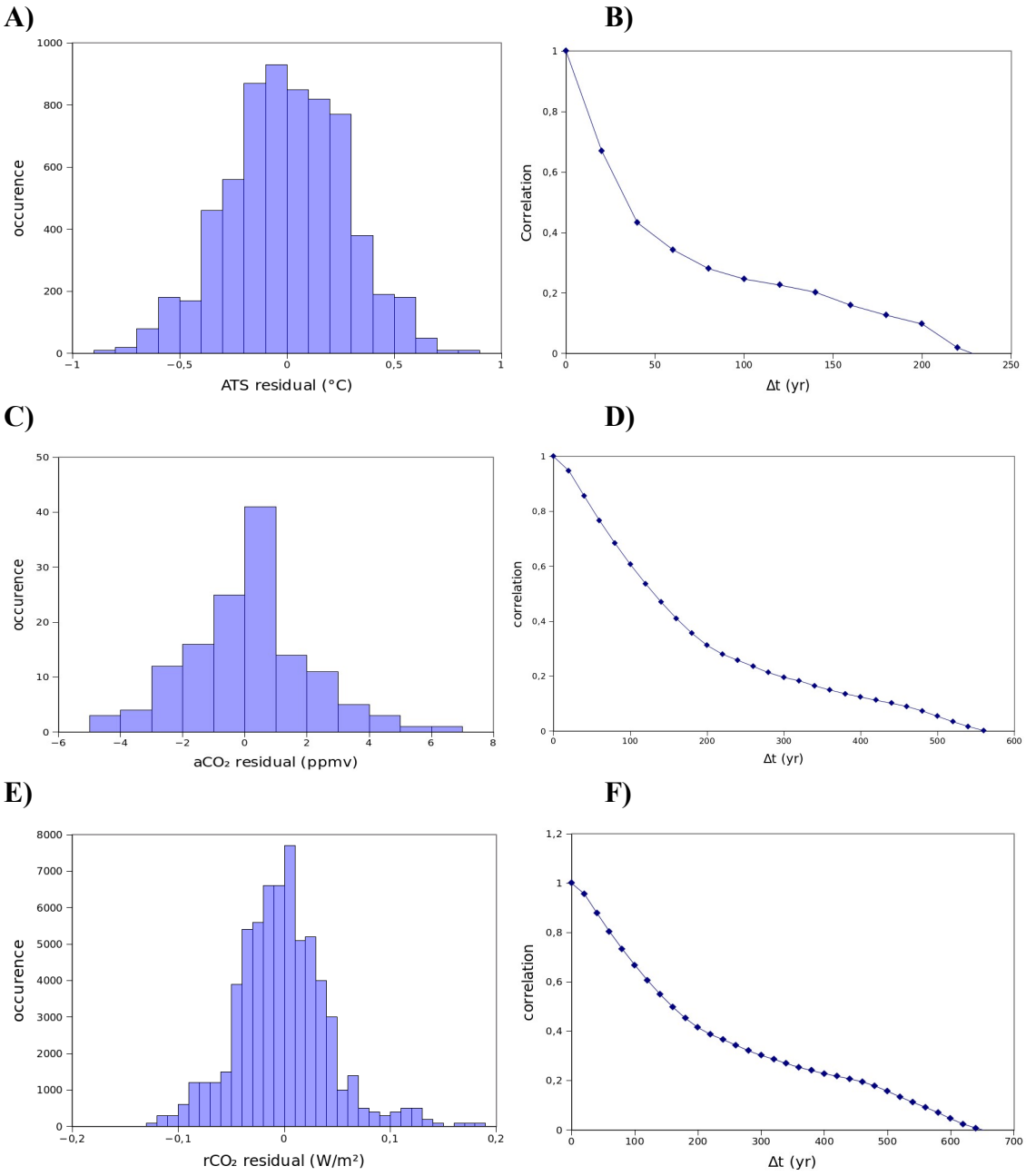

Fig. S6

Statistics on the residuals of the first best 6 points linear fit functions. **A)** Distribution of the AT residuals. σ=0.24°C. **B)** Correlation of the AT residuals as a function of the time distance. **C)** Distribution of the aCO_2 residuals. σ=1.94 ppmv. **D)** Correlation of the aCO_2 residuals as a function of the time distance.

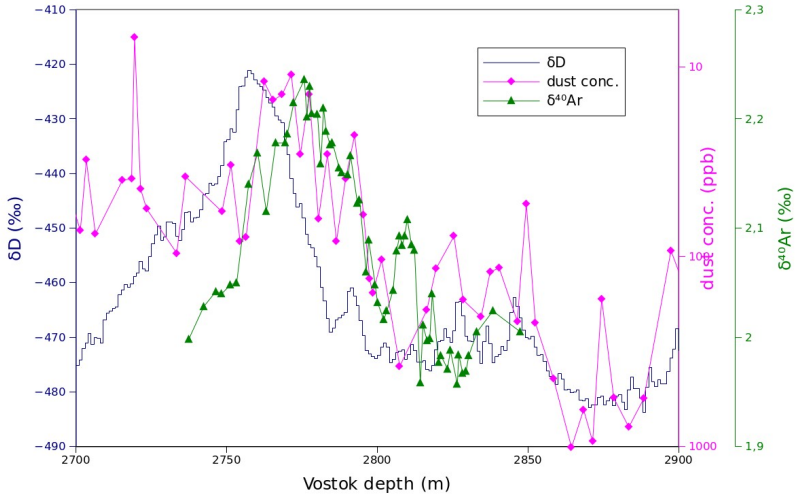

Fig. S7

δD *(31)*, dust concentration *(31)* and δ^{40}Ar *(32)* records of TIII in the Vostok ice core.

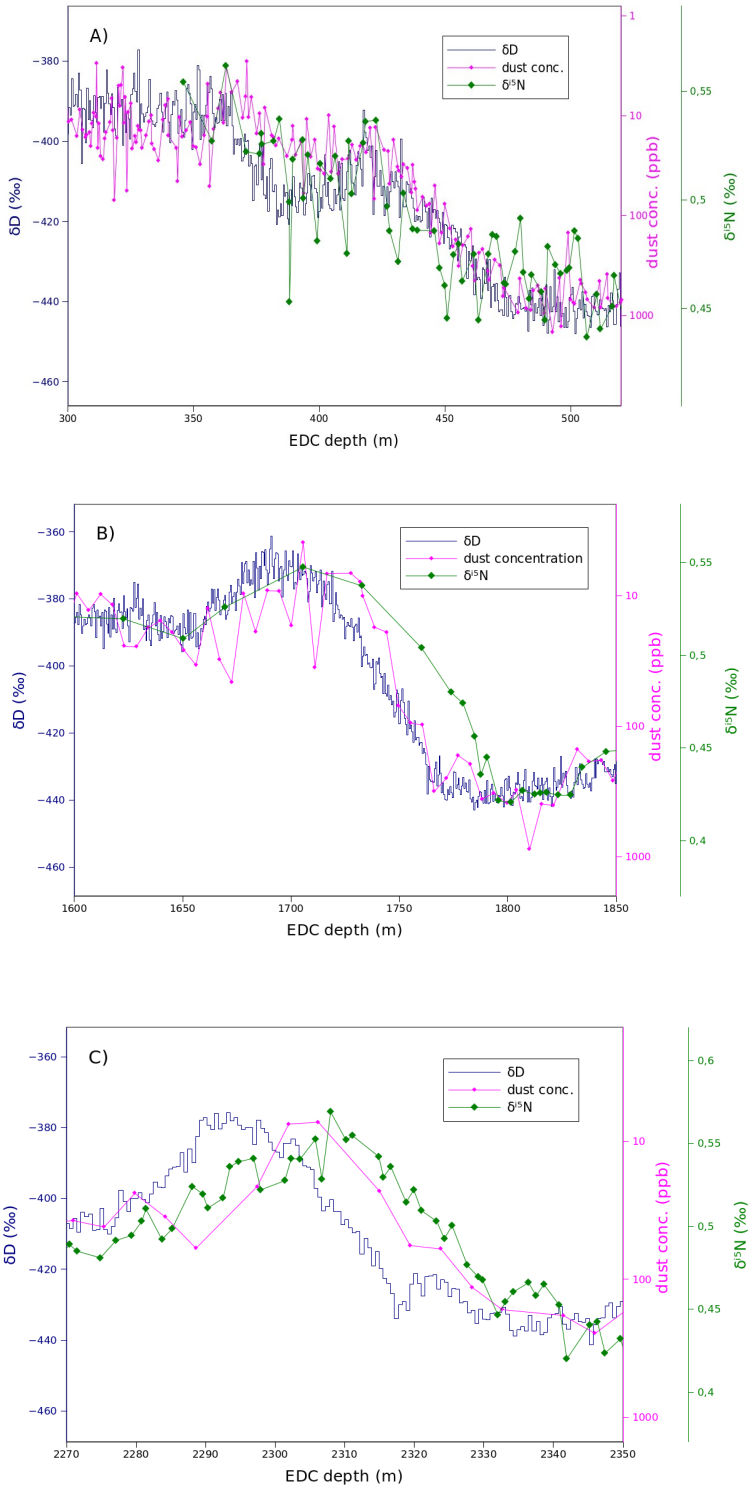

Fig. S8

δD *(16),* dust concentration *(33)* and $\delta^{15}N$ *(2)* records of TI (A), TII (B) and TIII (C) in the EDC ice core.

Tie points	EDC3 age (yr b1950)	Age this study (yr b1950)
$^{10}Be/^{14}C$ synchro	5280	5280
Onset of Holocene	11510	11600
Onset of Younger-Dryas	12810	12810
Onset of Bølling	14400	14680
Laschamp event	41200	41200

Table S1

Tie points between the EDC3 ice age scale and the ice age scale used in this study.

Ice core	δD or $\delta^{18}O$	Extension	References	Synchronization to EDC
EDC96	δD	0-45 kyr b1950	*(16)*	
EDC99	δD	45-800 kyr b1950	*(16)*	
DF	$\delta^{18}O$	0-335 kyr b1950	*(34)*	Table S3
Vostok	δD	0-415 kyr b1950	*(31)*	Table S4
TALDICE	δD	0-247 kyr b1950	*(35)*	*(35)* + Table S5
EDML	δD	0-140 kyr b1950	*(36)*	*(37)*

Table S2

Ice cores data used the construct the ATS stack.

Type	DF1 depth (m)	EDC99 detph (m)
surface	0	0
isotopic	356	360
isotopic	383	385
isotopic	419	419
isotopic	482	472
isotopic	610	585
isotopic	655	623
isotopic	671	635
isotopic	688	650
isotopic	745	700
isotopic	775	728
isotopic	792	740
isotopic	812	760
isotopic	854	800
isotopic	940	878
isotopic	966	900
isotopic	993	924
isotopic	1074	995
isotopic	1147	1062
isotopic	1188	1100
isotopic	1291	1200
volcanic	**1361.89**	**1265.1**
isotopic	1491	1391
isotopic	1543	1440
isotopic	1566	1457
isotopic	1734	1657
isotopic	1808	1751
volcanic	**1849.55**	**1796.3**
isotopic	1939	1888
isotopic	1953	1904
isotopic	1980	1933
isotopic	2001	1953

isotopic	2026	1980
isotopic	2066	2025
isotopic	2084	2045
volcanic	**2117.75**	**2086.6**
isotopic	2138	2107
volcanic	**2170.18**	**2150.9**
isotopic	2191	2177
isotopic	2226	2223
isotopic	2236	2235
isotopic	2278	2290
isotopic	2299	2322
isotopic	2333	2370
isotopic	2388	2442
isotopic	2401.5	2459
isotopic	2411	2470
isotopic	2420.5	2483
isotopic	2446.5	2513
isotopic	2485	2565
isotopic	2500	2592

Table S3

Tie points between the DF and EDC99 ice cores. Volcanic (labelled 'volcanic') tie points are from *(38)*, ice isotopic (labelled 'isotopic') tie points are from this study.

Type	VK depth (m)	EDC99 depth (m)
surface	0	0
isotopic	262	360
isotopic	287	385
isotopic	311	418
isotopic	357	472
isotopic	449	587
isotopic	467	605
isotopic	490	623
isotopic	499	636
isotopic	514	650
isotopic	540	670
isotopic	570	700
isotopic	596	729
isotopic	608	740
isotopic	625	759
isotopic	664	800
isotopic	773	878
isotopic	800	899
isotopic	920	996
isotopic	981	1040
isotopic	1010	1061
isotopic	1062	1101
isotopic	1192	1200
isotopic	1256	1245
isotopic	1450	1412
isotopic	1484	1440
isotopic	1783	1657
Volcanic	**1991.93**	**1804**
isotopic	2148	1888
isotopic	2177	1904
isotopic	2235	1933

isotopic	2275	1953
isotopic	2325	1980
isotopic	2402	2025
isotopic	2431	2045
Volcanic	**2501.9**	**2086.6**
isotopic	2531	2106
Volcanic	**2586.2**	**2150.9**
isotopic	2625	2177
isotopic	2679	2223
isotopic	2693	2235
isotopic	2760	2295
isotopic	2790	2322
isotopic	2827	2353
isotopic	2845	2368
isotopic	2900	2412
isotopic	2937	2442
isotopic	2962	2459
isotopic	2979.5	2470
isotopic	2998	2484
isotopic	3037	2513
isotopic	3102	2566
isotopic	3146	2602
isotopic	3215	2658
isotopic	3230	2674.5
isotopic	3241	2684
isotopic	3310	2750

Table S4

Tie points between the Vostok and EDC99 ice cores. Volcanic tie points are from *(38)*. Vostok depth as defined in *(31)*.

Type	TALDICE depth (m)	EDC99 depth (m)
isotopic	1160	800
isotopic	1220	880
isotopic	1256.5	942
isotopic	1282.5	997
isotopic	1303	1060
isotopic	1312	1100
isotopic	1332	1200
isotopic	1365	1390
isotopic	1374.5	1442
isotopic	1404	1658
isotopic	1440	1855
isotopic	1446	1889
isotopic	1463	1906
isotopic	1471	1935
isotopic	1477.5	1952.5
isotopic	1485	1981
isotopic	1493.7	2027
isotopic	1497	2048
isotopic	1508	2093
isotopic	1522.5	2170
isotopic	1528	2222
isotopic	1534	2235
isotopic	1545	2295
isotopic	1582	2500

Table S5

Isotopic tie points between the TALDICE and EDC99 ice cores.

LR04 age (yr b1950)	EDC99 depth (m)	EDC age (yr b1950)
0	116.609	3000
13050	452.439	16050
81250	1186.32	82300
105750	1444.53	106900
131950	1745.62	132800
198000	2075.97	198150
215400	2179.01	215500
227800	2229.28	227900
243450	2312.96	245600
286150	2442.81	290450
312450	2512.57	315900
335550	2594.45	337900
424600	2780.09	427250
490050	2841.57	488000
512000	2872.71	509750
533600	2905.15	530400
580750	2996.48	581900
622350	3037.96	628100
714000	3119.87	718750
743650	3138.55	740550
795500	3188.68	800150

Table S6

Synchronisation of the LR04 stack with EDC isotopic variations on the EDC3 age scale.

i	T_i AT (yr)	σ T_i AT (yr)	T_i aCO_2 (yr)	σ T_i aCO_2 (yr)	T_i rCO_2 (yr)	σ T_i rCO_2 (yr)
0	9000		9000		9000	
1	11684	31	11183	50	11199	59
2	12691	30	12747	73	12757	86
3	14688	42	14433	78	14533	112
4	17984	63	17993	59	18064	64
5	22000		22000		22000	

Table S7

Reconstructed break points of the 6 points linear fit procedure for AT, aCO_2 and rCO_2.

References and Notes

1. F. Parrenin *et al.*, *Clim. Past* **8**, 1239-1255 (2012).
2. G. B. Dreyfus *et al.*, *Quat. Sci. Rev.* **29**, 28-42 (2010).
3. G. Krinner, D. Raynaud, C. Doutriaux and H. Dang, *J. Geophys. Res.* **105**, 2059-2070 (2000).
4. F. Parrenin *et al.*, *Clim. Past* **3**, 485-497 (2007).
5. L. Loulergue *et al.*, *Nature* **453**, 383-386 (2008).
6. A. Svensson *et al.*, *Clim. Past* **4**, 47-57 (2008).
7. T. Blunier *et al.*, *Clim. Past* **3**, 325-330 (2007).
8. B. Stenni *et al.*, *Quat. Sci. Rev.* **29**, 146 - 159 (2010).
9. R. Bintanja, R. S. Van de Wal and J. Oerlemans, *Nature* **437**, 125-128 (2005).
10. L. E. Lisiecki and M. E. Raymo, *Paleoceanography* **20**, PA1003 (2005).
11. J. Jouzel and L. Merlivat, *J. Geophys. Res.* **89**, 11749-11757 (1984).
12. A. Tarantola, , Elsevier Sci., New York (1987).
13. N. Metropolis, A. Rosenbluth, M. Rosenbluth, A. Teller and E. Teller, *J. Chem. Phys.* **21**, 1087-1092 (1953).
14. W. Hastings, *Biometrika* **57**, 97-109 (1970).
15. F. Parrenin *et al.*, *Clim. Past* **3**, 243-259 (2007).
16. J. Jouzel *et al.*, *Science* **317**, 793-796 (2007).
17. V. Masson-Delmotte *et al.*, *Quat. Sci. Rev.* **29**, 113 - 128 (2010).
18. V. Masson-Delmotte *et al.*, *Clim. Past* **7**, 397-423 (2011).
19. L. C. Sime, E. W. Wolff, K. I. C. Oliver and J. C. Tindall, *Nature* **462**, 342-345 (2009).
20. T. Laepple, M. Werner and G. Lohmann, *Nature* **471**, 91-94 (2011).
21. F. Vimeux, V. Masson, J. Jouzel, M. Stievenard and J. R. Petit, *Nature* **398**, 410-413 (1999).
22. B. Stenni *et al.*, *Science* **293**, 2074-2077 (2001).
23. K. Kawamura *et al.*, *Nature* **448**, 912-917 (2007).
24. R. Uemura *et al.*, *Clim. Past* **8**, 1109-1125 (2012).
25. R. Winkler *et al.*, *Clim. Past* **8**, 1-16 (2012).
26. M. Siddall, G. A. Milne and V. Masson-Delmotte, *Earth Planet. Sci. Let.* **315-316**, 12 - 23 (2012).
27. V. Morgan *et al.*, *Science* **297**, 1862-1864 (2002).
28. A. Landais *et al.*, *Quat. Sci. Rev.* **25**, 49-62 (2006).
29. J. B. Pedro *et al.*, *Clim. Past* **7**, 671-683 (2011).
30. J. B. Pedro, S. O. Rasmussen and T. D. van Ommen, *Clim. Past* **8**, 1213-1221 (2012).
31. J. R. Petit *et al.*, *Nature* **399**, 429-436 (1999).
32. N. Caillon *et al.*, *Science* **299**, 1728-1731 (2003).
33. EPICA community members, *Nature* **429**, 623-628 (2004).

34. O. Watanabe *et al.*, *Nature* **422**, 509-512 (2003).
35. B. Stenni *et al.*, *Nature Geosci* **4**, 46-49 (2011).
36. null EPICA community members, *Nature* **444**, 195-198 (2006).
37. U. Ruth *et al.*, *Clim. Past* **3**, 475-484 (2007).
38. B. Narcisi, J. R. Petit, B. Delmonte, I. Basile-Doelsch and V. Maggi, *Earth Planet. Sci. Let.* **239**, 253-265 (2005).